Multidecadal Climate-induced Variability in Microseisms

Richard C. Aster
New Mexico Institute of Mining and Technology

Daniel E. McNamara
United States Geological Survey

Peter D. Bromirski
Scripps Institution of Oceanography

INTRODUCTION

Microseisms are the most ubiquitous continuous seismic signals on Earth at periods between approximately 5 and 25 s (Peterson 1993; Kedar and Webb 2005). They arise from atmospheric energy converted to (primarily) Rayleigh waves via the intermediary of wind-driven oceanic swell and occupy a period band that is uninfluenced by common anthropogenic and wind-coupled noise processes on land (Wilson *et al.* 2002; de la Torre *et al.* 2005). "Primary" microseisms (near 8-s period) are generated in shallow water by breaking waves near the shore and/or the nonlinear interaction of the ocean wave pressure signal with the sloping sea floor (Hasselmann 1963). Secondary microseisms occur at half of the primary period and are especially strongly radiated in source regions where opposing wave components interfere (Longuett-Higgins 1950; Tanimoto 2007), which principally occurs due to the interaction of incident swell and reflected/scattered wave energy from coasts (Bromirski and Duennebier 2002; Bromirski, Duennebier, and Stephen 2005). Coastal regions having a narrow shelf with irregular and rocky coastlines are known to be especially efficient at radiating secondary microseisms (Bromirski, Duennebier, and Stephen 2005; Shulte-Pelkum *et al.* 2004). The secondary microseism is globally dominant, and its amplitudes proportional to the square of the standing wave height (Longuett-Higgins 1950), which amplifies its sensitivity to large swell events (Astiz and Creager 1994; Webb 2006).

Microseisms have long been recognized as an indicator of large-storm intensity (Gilmore 1946; Gutenberg 1947; Gilmore and Hubert 1948). However, contributions from deep-water open-ocean storms are not generally significant in records from land-based seismometers (Bromirski and Duennebier 2002; Haubrich and McCamy 1969). Rather, microseism levels predominantly measure spatially distributed wave activity associated with wave interactions along coasts. The efficient propagation and ubiquity of short-period microseism Rayleigh waves (Bromirski, Duennebier, and Stephen 2005; Schulte-Pelkum *et al.* 2004; Bromirski 2001; Stehly *et al.* 2006), has also recently spurred their use in tomography (*e.g.*, Sabra *et al.* 2005; Shapiro *et al.* 2005).

DATA ANALYSIS

To examine global variability in microseism power at time scales ranging from days to decades, we utilize 1 sample/s continuous velocity time series from the Global Seismographic Network (GSN; figure 1; Butler *et al.* 2004) and its predecessor networks, the Seismic Research Observatory (SR; 1974–1993) and the High-Gain, Long-Period Network (HG; 1972–79). All data are vertical-component records retrieved from the Incorporated Research Institutions for Seismology (IRIS) Data Management System and/or from the U.S. Geological Survey (USGS) Albuquerque Seismological Laboratory (ASL). Deconvolving the instrument responses from the raw spectra provides calibrated globally distributed seismic records at periods greater than several seconds extending back as far as the early 1970s. The shorter-period part of the secondary microseism period band was excluded by analog filtering of some of the earlier (SR and HG) data. However, data available from the modern GSN collected since the late 1980s include the complete microseism at periods longer than approximately 3 s.

Microseism history is characterized using power spectral densities (PSDs). Specifically, PSDs for 1.5-hour 50% overlapping data segments are gathered to construct empirical probability density functions (PDFs) that statistically characterize longer time periods (McNamara and Buland 2004; figure 2). Earthquakes, of course, commonly generate high-amplitude surface waves in the period band that exceed microseismic background PSD levels by 60 dB or more. These transients are, however, very effectively suppressed in this analysis because they

doi: 10.1785/gssrl.79.2.194

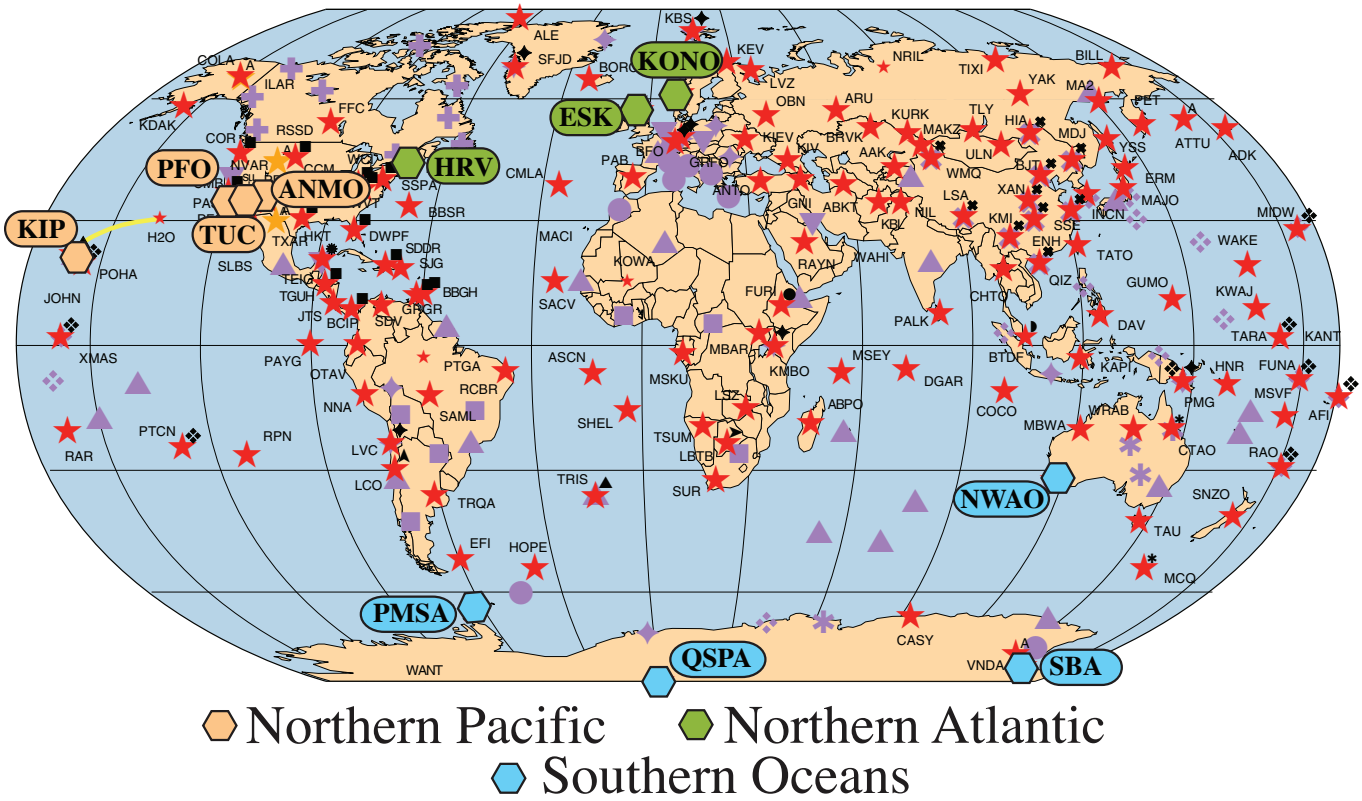

▲ **Figure 1.** Global Seismographic Network (Butler *et al.* 2004), as of 2007, with stations referred to here highlighted and geographically categorized. GSN affiliated stations are shown as purple symbols. Stations noted are: Oahu, Hawaii (KIP), Piñon Flat, southern California (PFO), Tucson, Arizona (TUC), Albuquerque, New Mexico (ANMO), Harvard, Massachusetts (HRV), Eskdalemuir, Scotland (ESK), Kongsberg, Norway (KONO), Narrogin, southwest Australia (NWAO), Palmer Station, Antarctica (PMSA), Scott Base, Antarctica (SBA), and South Pole (QSPA).

decay below microseism levels on time scales of hours, even for the largest events (Park *et al.* 2005), and thus affect a very small percentage of data segments.

Deep-water ocean swell propagates with group velocity $U = gT/(2\pi)$, where T is the wave period in seconds and g is the acceleration of gravity, so that characteristic 16-s swell will propagate at approximately 12.5 m/s and has long been known to commonly transit ocean basin–scale distances (*e.g.*, Munk *et al.* 1963; MacAyeal *et al.* 2006). To process seismic excitation arising from large swell events into seasonal-scale metrics, microseism levels were examined using median PSDs across 50% overlapping 36.525-day (deciyear) intervals for a global distribution of 11 long-running GSN stations (figures 1, 2, and 3A). To examine temporal evolution of microseism power, median PSD PDFs are integrated across the secondary (which is overwhelmingly dominant; figure 2) component of microseisms between 5.62 and 12.6 s period (figure 3B).

Regional associations between the secondary microseism power time series of figure 3B are revealed by correlation-based similarity analysis (Rowe *et al.* 2002; Sneath and Sokal 1973) (figure 4) across the common 12-year interval of 1 June 1994–1 July 2006. Microseism power in both the northern and southern hemispheres shows very strong (~ 20 dB at many stations) interannual variability driven by especially energetic swell occurring during respective winters. The annual periodic component of the power time series is characterized by fitting annual Fourier series coefficients to the 12-year common time series for the stations of figure 3 between 1 June 1994 and 31 May 2006 (figure 4).

DISCUSSION

Microseism power series correlate strongly with continent-scale station distribution (figure 4). Western U.S. stations (KIP, TUC, and ANMO) show a primarily Pacific association, and U.S. East Coast and northern European stations (ESK, HRV, and KONO) have relatively minor Atlantic associations. Deep Antarctic stations (SBA, SPA/QSPA) show strong association with each other, but are only weakly correlated with other coastal southern hemisphere stations (PMSA and NWAO). This degree of regionalization is comparable to that observed in studies utilizing meteorological buoy measurement of swell amplitude (Bromirski, Cayan, and Flick 2005). Both northern and southern hemisphere temperate latitude stations demonstrate especially strong annual periodicity, with annual power peaks that are within 10° in phase of their respective wave-year peaks, which are in turn within a few weeks of their respective winter solstices (using the reference date Jan. 1 to ascribe the

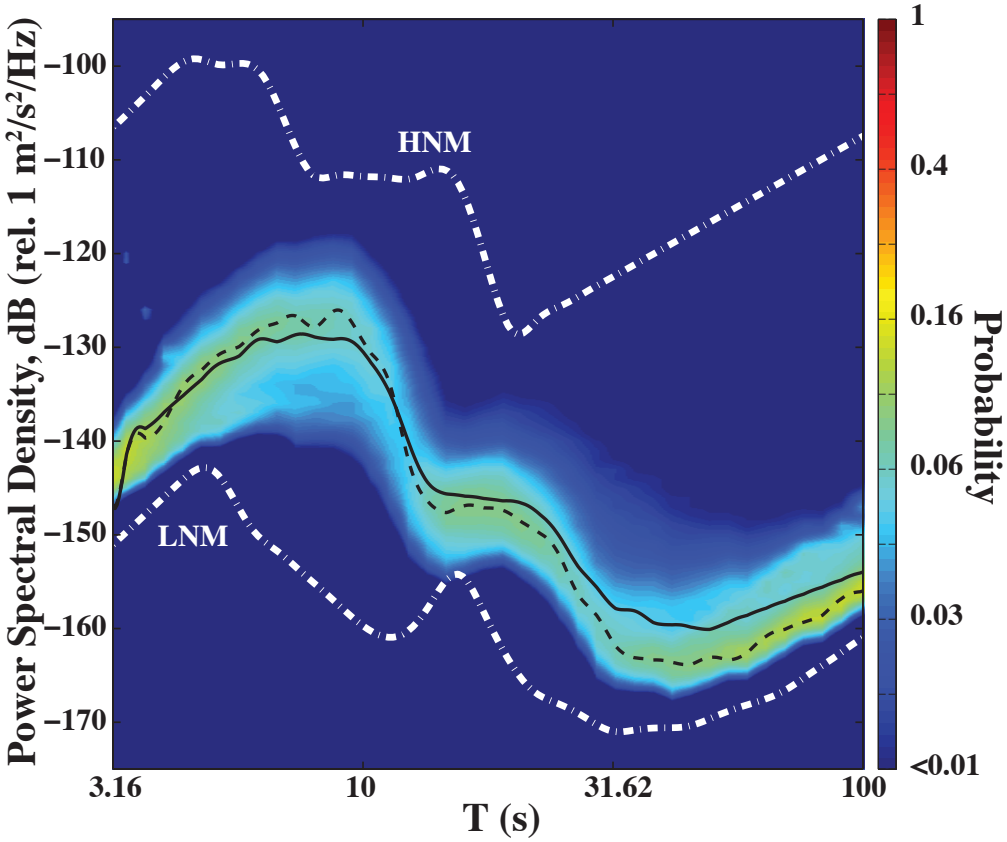

▲ **Figure 2.** Background seismic spectrum at Albuquerque, New Mexico (approximately 1,200 km from the California Pacific coast) for a 20-year period (1 June 1986 through 31 May 2006) characterized by a power spectral density (PSD) probability density function (PDF) using the method of McNamara and Buland (2004). The globally characteristic peaks near 8 and 16 s are the secondary (predominant) and primary microseisms, respectively. Median (solid) and mode (dashed) PDF curves are indicated, and dashed bounding curves show the globally estimated Global Seismographic Network low- and high-noise models (LNM; HNM; Peterson 1993). We compute power spectral density (PSD) using the algorithm used to develop the GSN LNM. This figure is constructed using 88,865 1.5-hr, continuous, and overlapping (50%) 1 sample/s time series segments. All data are included; there is no removal of earthquakes, system transients, and/or data glitches. The instrument transfer function is removed from each segment, yielding ground acceleration for easy comparison to the LNM. Each 1.5-hour-long time series segment is divided into 13 subsegments, overlapping by 75%. Each subsegment is processed by: 1) removing the mean, 2) removing the long period trend, 3) tapering using a 10% sine function, 4) applying the Fourier transform, 5) constructing a PSD estimate for the segment via Welch's method (*e.g.*, Oppenheim and Schafer 1975). The PDF for the entire period is then constructed by gathering PSDs in the following manner: 1) binning periods in 1/8 octave intervals, 2) binning power in 1 dB intervals. Each period-power bin is subsequently normalized by the number of contributing segments to construct an empirical PDF. The density function displays ~ 20 dB of microseism power variability driven by midsummer wave minima and midwinter wave maxima, primarily in the northern Pacific Ocean.

phases of the periodic microseism components in figure 4). PMSA, on the Antarctic Peninsula, also shows an apparent wave-year related annual phase, but the annual periodicity is very low (a periodic fit variance reduction of only $V = 11\%$). We attribute the notably aperiodic PMSA microseism to the strong influence of local storms in the tempestuous Antarctic Peninsula region throughout the year. Deep Antarctic stations (SBA and QSPA) show strong annual periodicity ($V > 70\%$) but have annual microseism peak phases relative to Jan. 1 of 83° and 92°, respectively, which we suspect are attributable to undetermined processes associated with seasonal sea ice.

Microseism power time series show significant interannual variability in both the primary and secondary period bands, with aperiodic components accounting for between 89% (PMSA) to 25% (KIP) of the total signal energy (figure 4). Near-coastal stations (*e.g.*, PFO, KIP, NWAO, ESK, HRV, PMSA, TUC) exhibit short-term aperiodic power variations that reflect greater local sensitivity to specific storms. The mid-Pacific oceanic island site KIP exhibits exceptionally high microseism levels and the most periodically predictable signal over this observational interval ($V = 75\%$; figure 4), indicating that the long coastline of the Hawaiian Islands provides exceptional integrative coupling of Pacific wave activity into microseismic energy. The northern Pacific/western United States power series affinity (figure 4) of KIP indicates that this energy primarily originates from northern Pacific winter storms. During

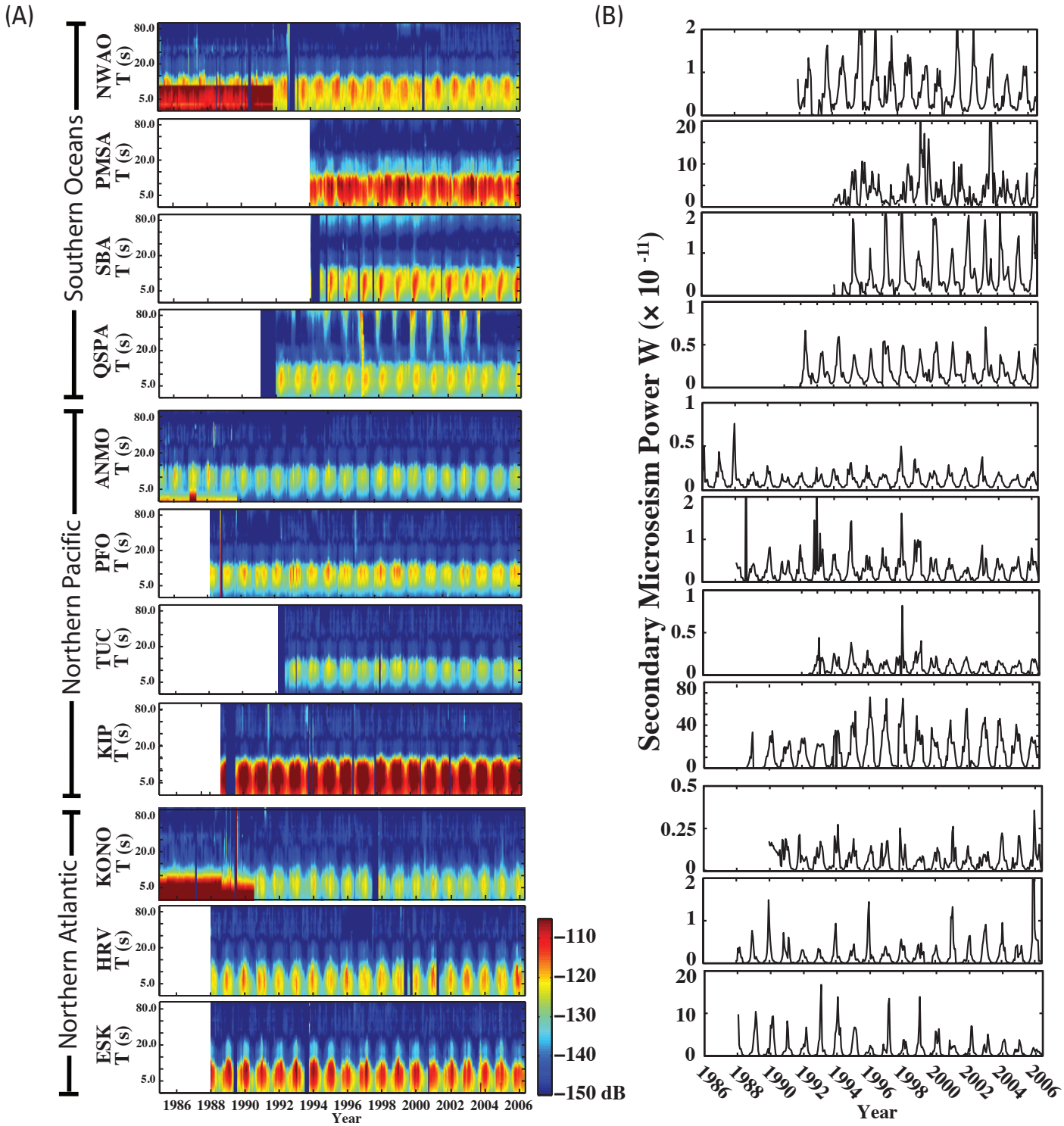

▲ **Figure 3.** (A) Velocity PSD PDF medians (figure 2) as a function of year (Jan. 1) and period, T, calculated using 50% overlapping deciyear (36.525-day) time series, and arranged by global locale (figure 1). Solid blue swaths signify station downtime, and red, short-period blocks in the oldest data from NWAO, ANMO, and KONO are due to irreversible early short-period microseismic filtering. (B) Velocity power levels in the predominant secondary (figure 2) microseism band obtained from integrating median PSD values (figure 3) between 5.62 and 12.6 s period in 50% overlapping deciyear time windows, displaying long-term annual and other power trends. Power is physically equivalent to that imparted to a 2 kg mass by vertical ground motion. Note that power axis scales are four times greater at Kipapa (Oahu) Hawaii (KIP) and ten times greater for Palmer Station, Antarctica (PMSA) and Eskdalemuir, Scotland (ESK), which experience exceptionally high microseism levels typical of oceanic islands (Peterson 1993).

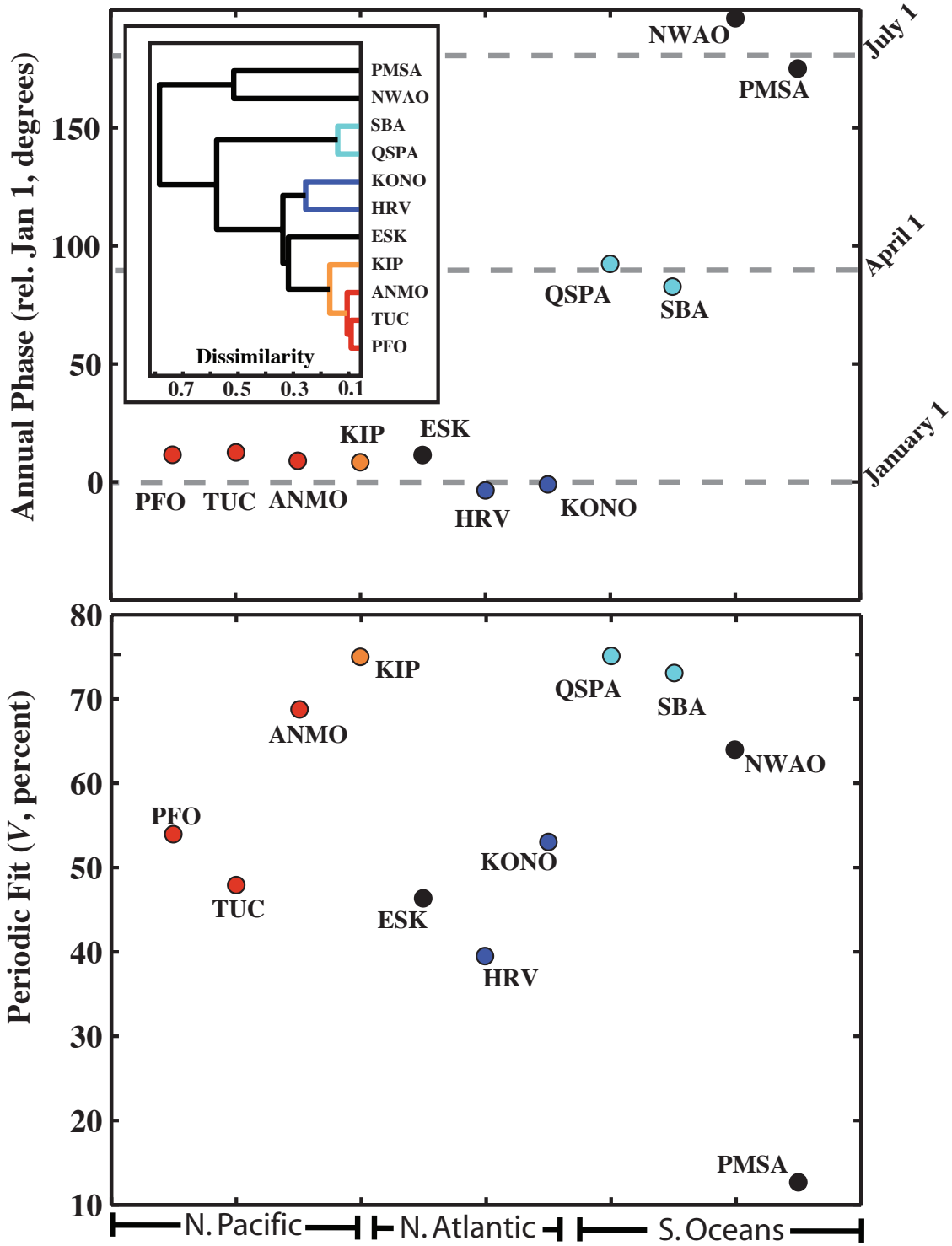

▲ **Figure 4.** Annual phase (relative to 1 January; top) and periodic fit (bottom) for secondary microseism power series (figure 3B) using five Fourier terms for June 1994 through June 2006. Microseism power level time series predictability via annual fundamental and harmonic terms is expressed as the variance reduction, $V = (||\mathbf{d}||^2 - ||\mathbf{d} - \mathbf{d}_{pred}||^2)/||\mathbf{d}||^2$, where $\mathbf{d}$ is the data and $\mathbf{d}_{pred}$ is the prediction using the fundamental and its first four harmonics (fitting higher harmonics gave no further improvement). The phase of annual cycle relative to the beginning of the calendar year is parameterized by the phase of the fundamental (1-year) Fourier term. *Inset*: Regional secondary microseism affinities characterized using correlation-based classification of demeaned and standard-deviation-normalized power time series (figure 3B; June 1994–June 2006). Dendrogram construction utilized the group average (unweighted average distance) hierarchical method (Sneath and Sokal 1973) using the demeaned power time series and a dissimilarity measure of $1 - c$, where c is the zero-lag cross-correlation coefficient.

strong El Niño/La Niña episodes, such storms are intensified in frequency and size (particularly in the Gulf of Alaska) and generate exceptionally large swell in Hawaii and along the western coast of North America (Bromirski, Duennebier, and Stephen 2005; Allan and Komar 2002). The multiyear peaks in microseism energy in 1997–98 and 2002–04 at KIP, ANMO, PFO, and TUC correlate with increased northeast Pacific storminess during El Niño Southern Oscillation (ENSO) cycles (Hoerling and Komar 2002; McPhaden *et al.* 2006) during these periods. The largest energies for these northern Pacific stations occur during the 1997–98 El Niño northern hemisphere wave year, in general agreement with studies of wave heights in the eastern northern Pacific measured by NOAA buoys (Bromirski, Cayan, and Flick 2005).

The longest continuously running seismic stations present the possibility of examining microseism variations in the multidecade range at time resolutions as fine as the three–five-day synoptic swell variability from individual storms (Bromirski, Flick, and Graham 1999). Figure 5 shows such microseism power levels for ANMO from 1 January 1978 through 31 May 2006 using 4.56-day (1/80 of a year) 50% overlapping median PSD PDF windows. Earlier instrumentation prevents analysis of the shorter-period microseism at this station; however, the 10–20-s period band is resolved and allows for analysis across a 28.5-year interval at these longer periods, which is dominated by secondary microseism signals arising from exceptionally high-wind and large-fetch northern Pacific winter storms. ANMO microseism power levels generally co-vary with wave heights along the southern California coast, as measured at a NOAA buoy near Point Arguello, (figures 5C and 5D; we raise the measured wave heights to the fourth power because the seabed forcing by the secondary microseism mechanism is predicted to be proportional to the square of wave height [Longuett-Higgins 1950] and because we are comparing the buoy-estimated wave measurements to microseism power, which is, in turn, proportional to the square of the source forces), with the annualized wave and microseism power shown in figures 5D and 5E. Both seismic and buoy time series show notably high amplitudes during the 1983 El Niño and the 1997–99 ENSO, with the 1983 episode being relatively transient in its microseism and wave influence because of the lack of subsequent strong La Niña. During these exceptional years, both microseism energy and the annualized wave forcing are larger than median years by a factor of two to three. In contrast, the more modest 1988–89 ENSO exhibits lower levels of both wave and microseismic energy (60–80% of the other observed ENSO cycles).

Microseism and buoy time series during the 1997–2000 period, which includes a very prominent ENSO cycle, are shown in figure 6. The maximum of the correlation function, C, between the 2.28-day demeaned seismic and buoy measurements across the 22-year common data interval (northern hemisphere wave years 1982 through 2004) is 0.62 (figure 6) with the interpolated maximum occurring essentially at zero lag (the wave record lags the microseism record by 0.5 ± 1.2 d at the 95% points of the cross-correlation peak). The annual side lobes of the cross-correlation function, corresponding to misaligned years, have maxima of $C < 0.2$. This degree of correlation, despite the substantial distance between the coast and the inland continental seismometer site (1,280 km), reflects the integrative sensitivity of ANMO to microseism sources along the Pacific coast of North America (figure 4), including more northerly Pacific storms that produce relatively low-amplitude waves along the southern California coast (Allan and Komar 2002). Peaks in the two time series correlate strongly in time with effectively zero lag, but show variable amplitude ratios (by a factor of two or more for strong storms; figure 6) that are indicative of secondary microseism generation conditions associated with specific swell episodes sensed by the (point measurements of the) ocean buoys. This variability between specific events is likely to arise from several factors including the angle of swell propagation with respect to the coast, the associated length of coastline nearly simultaneously illuminated by a swell event (reflective of the spatial continuity of the incident swell), and the coastal morphology determining the combined reflected/scattered swell directional spectrum (Bromirski and Dunnebier 2002; Bromirski 2001).

Microseism analysis at long-running seismic observatories produces quantitative wave intensity metrics with spatiotemporal wave integrating characteristics that complement more localized (*e.g.*, buoy-based) measurements. The degree to which microseisms at specific stations are sensitive to local versus regional-scale swell is dependent on geography. This work indicates that the greatest degree of integration will occur for either of two end-member geographic scenarios. The first scenario is at oceanic islands, which have broad exposure to swell propagating from multiple source regions, and where microseisms are generated at regional to local distances from the station (*e.g.*, Hawaii). The second scenario is at interior continental sites that are sensitive to multiple near-coastal microseism source zones that radiate Rayleigh waves over regional to teleseismic distances (*e.g.*, stations in interior North America or Antarctica). Although continental interior sites have much lower microseism energies than oceanic island and near-coastal stations (*e.g.*, the annualized energies at ANMO are approximately 200 times lower than at KIP; figure 3B), microseisms are easily resolvable even at these quietest sites (Peterson 1993; Butler *et al.* 2004). Microseism metrics present novel constraints on sea roughness and climate in especially remote areas, such as Antarctica, where other data are rare or absent, and potentially offer the longest-running instrumental records of wave climate. Enhanced efforts to digitize analog records from the longest established seismological observatories offer the possibility of establishing microseism wave climate metrics back to the mid-20th century (Grevemeyer *et al.* 2000), and perhaps earlier, and present a unique opportunity for quantitatively characterizing regional and global storm behavior and energies at the centennial time scale. Because of the sensitivity of microseisms to large waves, further investigation is warranted to test predictions and corroborate other observables reflecting a possible climate change–induced increase in extreme storms (*e.g.*, Knutson *et al.* 1998; Meehl *et al.* 2000; Emanuel 2005; Bromirski *et al.* 2005; McNamara *et al.* 2007).

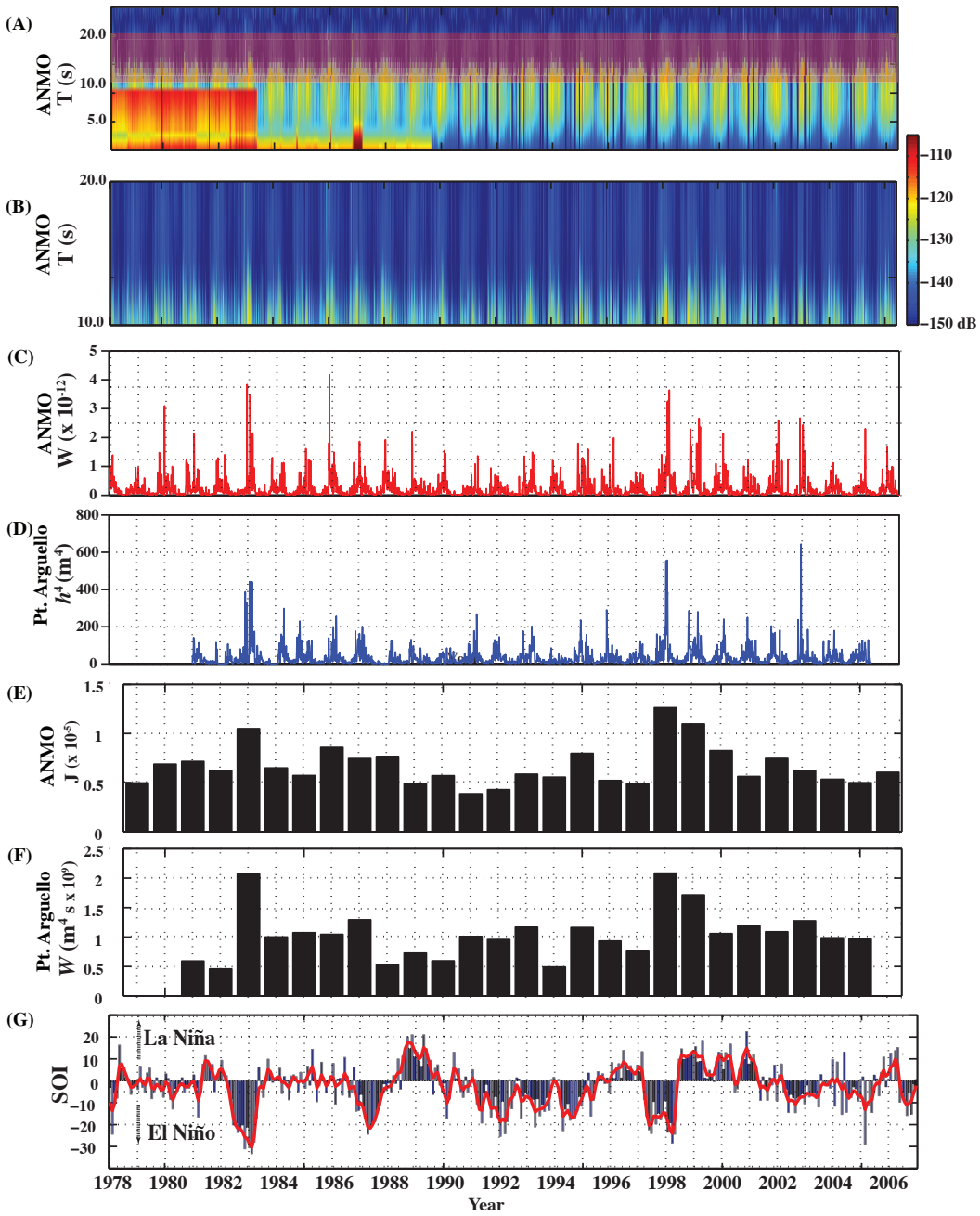

▲ **Figure 5.** (A) ANMO (1 January 1978–31 May 2006) PSD PDF medians evaluated using 50% overlapping 4.56-day windows. (B) Detailed view of (A) showing large storm secondary microseisms between 10 to 20 s (period swath shown in 3A). (C) Power levels obtained from integrating the data in (B). Note that this period band is well recovered throughout the observation period. (D) 4.56-day averages of hourly wave heights, *h*, between 1 January 1981 and 31 December 2005, raised to the fourth power, collected by NOAA buoy 46023 located off Point Arguello, California, between 1 January 1981 and 31 July 2005, with some data gaps filled in by nearby southern California buoys 46011 and 46053 (Bromirski, Cayan, and Flick 2005). The great-circle separation between ANMO and buoy 46023 is approximately 1280 km. (E) Wave-year annualized (1 June–31 May) ANMO microseism energy between 10 and 20 s. (F) Comparative wave forcing, *W* (integral of the wave height to the fourth power). E and F were calculated from the data of C and D, respectively. (G) El Niño Southern Oscillation Index (*e.g.*, Trenberth 1997) (SOI; a normalized measure of the atmospheric pressure difference between Tahiti and Darwin, Australia) in monthly (blue) and five-month moving Hamming window-averaged (red) values between January 1978 and January 2007. Note the associations between SOI excursions and microseism-associated wave energy during this period for this northern Pacific affinity station (figure 4), particularly during the strong El Niño of 1983 and the strong El Niño/La Niña cycle of 1997–99, which were associated with exceptionally strong Pacific storms and swell along the western coast of North America (Hasselmann 1963; Bromirski, Cayan, and Flick 2005; Allan and Komar 2002; McPhaden *et al.* 2006).

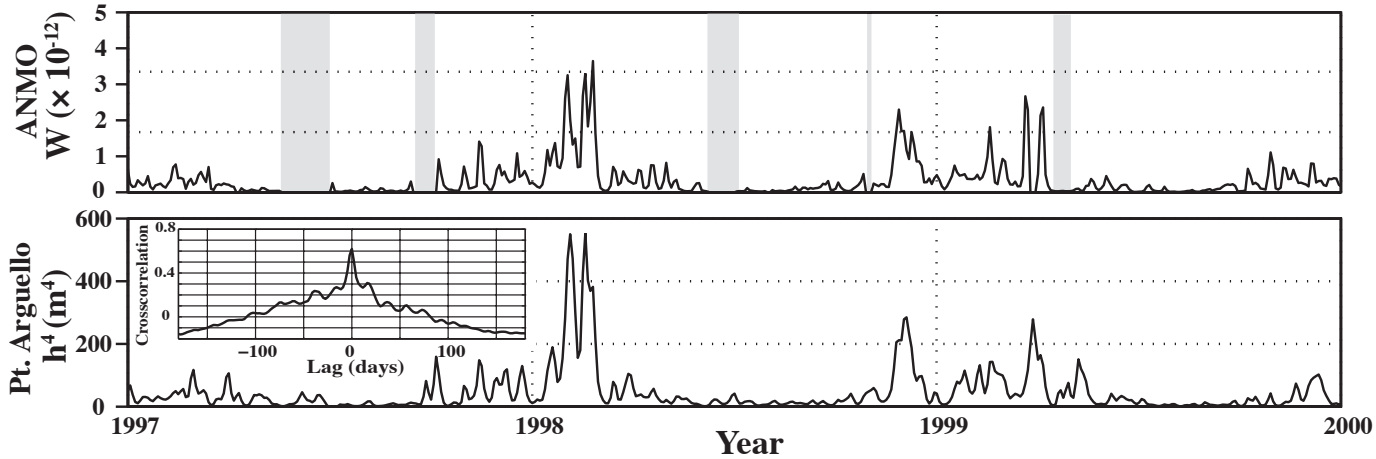

▲ **Figure 6.** Microseism power (10–20 s) and Point Arguello wave forcing time series, showing the 1997–99 El Niño/La Niña cycle (figure 5). Intermittent ANMO data outages are indicated in gray. The general character of the association is that of consistent peak correlations with variable relative amplitude levels. *Inset*: Cross-correlation function central maximum for the complete overlapping microseism/buoy data period of figure 5.

ACKNOWLEDGMENTS

The Global Seismographic Network (GSN) is a cooperative scientific facility operated jointly by the Incorporated Research Institutions for Seismology (IRIS), the United States Geological Survey (USGS), and the National Science Foundation (NSF). The facilities of the IRIS Data Management System (DMS), and specifically the IRIS Data Management Center, were used for access to waveform and metadata required in this study. The IRIS DMS is funded through the NSF and specifically the GEO Directorate through the Instrumentation and Facilities Program of NSF under Cooperative Agreement EAR-0004370. Additional support for P. Bromirski was provided by the California Department of Boating and Waterways. Key assistance was provided by the USGS Albuquerque Seismological Laboratory, especially L. Gee and C. Hutt. The authors also thank USGS internal reviewers J. Love and C. Hutt for their insights and thoughtful comments.

REFERENCES

Allan, J., and P. Komar (2002). Extreme storms on the Pacific Northwest coast during the 1997–1998 El Niño and 1998–1999 La Niña. *Journal of Coastal Research* **18**, 175–193.

Astiz, L., and K. Creager (1994). Geographic and seasonal variations of microseismic noise. *EOS, Transactions, American Geophysical Union* **75**, 419.

Bromirski, P. (2001). Vibrations from the "perfect storm." *Geochemistry, Geophysics, and Geosystems* **2**, 2000GC000119.

Bromirski, P., D. Cayan, and R. Flick (2005). Wave spectral energy variability in the northeast Pacific. *Journal of Geophysical Research* **110**, doi:10.1029/2004JC002398.

Bromirski, P., and F. Duennebier (2002). The near-coastal microseism spectrum: Spatial and temporal wave climate relationships. *Journal of Geophysical Research* **107**, doi:10.1029/2001JB000265.

Bromirski, P., F. K. Duennebier, and R. E. Stephen (2005). Mid-ocean microseisms. *Geochemistry, Geophysics, and Geosystems* **6**, Q04009, doi:10.1029/2004GC000768.

Bromirski, P. D., R. E. Flick, and N. Graham (1999). Ocean wave height determined from inland seismometer data: Implications for investigating wave climate changes in the Northeast Pacific. *Journal of Geophysical Research* **104**, 20,753–20,766.

Butler, R., T. Lay, K. Creager, P. Earle, K. Fischer, J. Geherty, G. Laske, B. Leith, J. Park, M. Ritzwoller, J. Tromp, and L. Wen (2004). The Global Seismographic Network surpasses its design goal. *EOS, Transactions, American Geophysical Union* **85** (23), 225–232.

de la Torre, T., and A. Sheehan (2005). Broadband seismic noise analysis of the Himalayan Nepal Tibet Seismic Experiment. *Bulletin of the Seismological Society of America* **95**, 1,202–1,208.

Emanuel, K. (2005). Increasing destructiveness of tropical cyclones over the past 30 years. *Nature* **436**, 686–688.

Gilmore, M. (1946). Microseisms and ocean storms. *Bulletin of the Seismological Society of America* **36**, 89–119.

Gilmore, M., and W. Hubert (1948). Microseisms and Pacific typhoons. *Bulletin of the Seismological Society of America* **38**, 195–228.

Grevemeyer, I., R. Herber, and H. Essen (2000). Microseismological evidence for a changing wave climate in the northeast Atlantic Ocean. *Nature* **408**, 349–352.

Gutenberg, B. (1947). Microseisms and weather forecasting. *Journal of Meteorology* **4**, 21–28.

Hasselmann, K. (1963). A statistical analysis of the generation of microseisms. *Reviews of Geophysics* **1**, 177–210.

Haubrich, R. A., and K. McCamy (1969). Microseisms: Coastal and pelagic sources. *Reviews of Geophysics* **7**, 539–571.

Hoerling, M. P., and A. Komar (2002). Atmospheric response patterns associated with tropical forcing. *Journal of Climate* **15**, 2,184–2,203.

Kedar, S., and F. Webb (2005). The ocean's seismic hum. *Science* **307**, 682–683.

Knutson, T., R. Tuleya, and Y. Kurihara (1998). Simulated increase of hurricane intensities in a C02-warmed climate. *Science* **279**, 1,018–1,021, doi: 10.1126/science.279.5353.1018.

Longuett-Higgins, M. S. (1950). A theory of the origin of microseism. *Philosophical Transactions of the Royal Society of London*, Series A, Mathematical and Physical Sciences, **243**, 1–35.

MacAyeal, D., E. Okal, R. Aster, J. Bassis, K. Brunt, L. Cathles, R. Drucker, *et al.* (2006). Transoceanic wave propagation links iceberg calving margins of Antarctica with storms in tropics and northern hemisphere. *Geophysical Research Letters* **33**, L17502, doi:10.1029/2006GL027235.

McNamara, D., R. Aster, P. Bromirski, C. Hutt, and L. Gee (2007). Seismological evidence for increasing oceanic storm intensity. *EOS,*

Transactions, American Geophysical Union **88**(52) Fall Meeting Supplement.
McNamara, D., and R. Buland (2004). Ambient noise levels in the continental United States. *Bulletin of the Seismological Society of America* **94**, 1,517–1,527.
McPhaden, M., S. Zebiak, and M. Glanz (2006). ENSO as an integrating concept in Earth science. *Science* **314**, 1,740–1,745.
Meehl, G., T. Karl, D. Easterling, S. Changnon, R. Pielke, D. Chagnon, and J. Evans *et al.* (2000). An introduction to trends in extreme weather and climate events: Observations, socioeconomic impacts, terrestrial ecological impacts, and model projections. *Bulletin of the American Meteorological Society* **81**, 413–416.
Munk, W. H., G. Miller, F. Snodgrass, and N. Barber (1963). Directional recording of swell from distant storms. *Philosophical Transactions of the Royal Society of London*, Series A, Mathematical and Physical Sciences **255**, 505–584.
Oppenheim, A. V., and R. Schafer (1975). *Digital Signal Processing.* Englewood Cliffs, NJ: Prentice-Hall.
Park, J., R. Butler, K. Anderson, J. Berger, H. Benz, P. Davis, R. Hutt, C. McCreery, T. Ahern, G. Ekstrom, and R. Aster (2005). Performance review of the Global Seismographic Network for the Sumatra-Andaman megathrust earthquake. *Seismological Research Letters* **76**, 329–341.
Peterson, J. (1993). *Observation and Modeling of Seismic Background Noise*. USGS Technical Report 93-322.
Rowe, C. A., R. C. Aster, B. Borchers, and C. J. Young (2002). An automatic, adaptive algorithm for refining phase picks in large seismic data sets, Part I: Technique. *Bulletin of the Seismological Society of America* **92**, 1,660–1,674.
Sabra, K., P. Gerstoft, P. Roux, W. Kuperman, and M. Fehler (2005). Extracting time-domain Green's function estimates from ambient seismic noise. *Geophysical Research Letters* **32**, L03310, doi:10.1029/2004GL021862.
Schulte-Pelkum, V., P. S. Earle, and F. L. Vernon (2004). *Geochemistry, Geophysics, and Geosystems* **5** doi:10.1029/2003GC000520
Shapiro, N. M., M. Campillo, L. Stehly, and M. Ritzwoller (2005). High-resolution surface-wave tomography from ambient seismic noise. *Science* **307**, 1,615–1,618.
Sneath, P., and R. Sokal (1973). *Numerical Taxonomy*. San Francisco: W.H. Freeman & Co.
Stehly, L., M. Campillo, and N. Shapiro (2006). A study of the seismic noise from its long-range correlation properties. *Journal of Geophysical Research* **111** (B10), 1–12, doi:10.1029/2005JB004237.
Tanimoto, T. (2007). Excitation of microseisms. *Geophysical Research Letters* **34**, L05308, doi:10.1029/2006GL029046.
Trenberth, K. (1997). The definition of El Niño. *Bulletin of the American Meteorological Society* **78** (12), 2,771–2,777.
Webb, S. (2006). The Earth's "hum" is driven by ocean waves over the continental shelves. *Nature* **445**, 754–756, doi:10.1038/nature05536.
Wilson, D., J. Leon, R. Aster, J. Ni, J. Schlue, S. Grand, S. Semken, S. Baldridge, and W. Gao (2002). Broadband seismic background noise at temporary seismic stations observed on a regional scale in the southwestern United States. *Bulletin of the Seismological Society of America* **92**, 3,335–3,341.

Department of Earth and Environmental Science
Geophysical Research Center
New Mexico Institute of Mining and Technology
Socorro, New Mexico 87801 USA
aster@ees.nmt.edu
(R.A.)

U.S. Geological Survey
1711 Illinois St.
Golden, Colorado 80401 USA
mcnamara@usgs.gov
(D.M.)

Scripps Institution of Oceanography
Integrative Oceanography Division 0209
9500 Gilman Drive
Scripps Institution of Oceanography
La Jolla, California 92093-0209 USA
pbromirski@ucsd.edu
(P.B.)